Refinement of Near-Surface P and S Wave Velocities in the SCEC 3D Velocity Model Using 3D Waveform Modeling

Tracy H. Pattelena
UC Santa Cruz, Santa Cruz, CA 95064

Kim B. Olsen
Institute for Crustal Studies, UC Santa Barbara, Santa Barbara, CA 93106

August 30, 2000

Abstract

An important part of ground motion studies opts to predict full theoretical seismograms for an earthquake at a given site. Our study focuses on the ground motion in a portion of the San Fernando Valley (SFV) where control on the near-surface S wave velocity, a critical parameter for accurate prediction of strong ground motion, is mostly indirect and in many areas not well constrained. We use 1-Hz 3D finite-difference simulations to propagate waves for a M_L=5.1 Northridge aftershock through two 10 km by 10 km by 5 km models of the SFV subsurface: (1) a subset of the SCEC southern California reference 3D seismic velocity model (version 2.0), and (2) model 1 modified with slower velocities in the near-surface material taken from a tomographic model. Model 2 contains near-surface P and S velocities up to 70% and 50% less than those of model 1, respectively, in the upper 500 m. Compared to the response of model 1, the tomographically refined model (2) generates peak ground velocities (PGV) and cumulative kinetic energies (CKE) up to a factor of two in localized areas of the model. While the synthetics for model 2 improve the fit to data at the five stations only slightly, our simulations suggest that version 2.0 of the SCEC velocity model is not complex enough to reproduce the 1-Hz duration and peaks in the SFV basin.

Introduction

One of the most important missions of the Southern California Earthquake Center is to promote earthquake hazard reduction. This mission is generally accomplished through ground motion studies, which opt to predict full theoretical seismograms for an earthquake at a given site. However, prediction of strong ground motion in the greater Los Angeles area

is by no means an easy task. The complex geology (see Wright, 1991) surely influences site response as does the low velocity material and geometry and structure of its deep sedimentary basins (see Boore, 1972; Joyner *et al.,* 1981; Vidale and Helmberger, 1988; Khain *et al.,* 1991; Borcherdt and Glassmoyer, 1992; Su *et al.,* 1992; Olsen *et al.,* 1995; Olsen and Archuleta, 1996; Hartzell *et al.,* 1997; Olsen, 2000). Estimates are further complicated by local focusing effects (Gao *et al.,* 1996; Alex and Olsen, 1998; Graves *et al.,* 1998) and linear versus nonlinear sediment response (Field *et al.,* 1997). Furthermore, since the shallow S wave impedance plays an important role in determining ground motion amplification (Day 1996; Anderson *et al.,* 1996), it is especially important to use as accurate as possible estimates of the S-wave velocity (V_s) in the ground motion estimates.

In cooperation with the Southern California Earthquake Center (SCEC), Magistrale *et al.* (2000) have produced version 2.0 of the SCEC southern California reference 3D seismic velocity model (herein referred to as the "SCEC reference model"). This reference model consists of detailed, rule-based representations of the major southern California basins embedded in a 3D crustal model. Data for the basins were compiled from geological, geophysical, and geotechnical data. P wave velocity (V_p) and V_s in the near-surface down to 200 m depth are constrained by geotechnical borehole data in the basins below Los Angeles and the San Fernando Valley. Where unknown, V_s is calculated from V_p and Poisson's ratio (σ). Such a model is useful for strong ground motion estimation. Our study focuses on the ground motion in a portion of the SFV (see Fig. 1), where control on the near-surface S wave velocity, a critical parameter for accurate prediction of strong ground motion, is mostly indirect and in many areas not well constrained.

For this study, we extracted a 10 km (East-West) by 10 km (North-South) by 5 km (ver-

tical) subset from the SFV portion (outlined by green rectangle in Fig. 1) of the latest SCEC reference model available at the SCEC Data Center website at http://www.scecdc.scec.org. Isovelocity surfaces of this subset show $V_s \leq 500$ m/s down to 100 m depth in some areas and $V_s \leq 1000$ m/s down to 870 m depth in the soft soils and sediments of the basin (see Fig. 2). We also incorporate results from a recent study by Pattelena *et al.* (1998) in which active-source industry data collected in our area of study were processed to produce three P wave velocity models at 50 m grid spacing for the upper 500 m of crust. These profiles are SFV-11, SFV-08, and SFV-12 (see Fig. 1 for location). Additionally, one of the three profiles, SFV-12, had S wave arrivals with a resolution sufficient for an S wave velocity model to be generated. Since all three tomographic models show similar, unusually slow V_p in the near-surface material of the SFV basin, we chose to work only with tomographic model SFV-12. A strong limitation of this, however, is that the V_s values from model SFV-12 are assumed to also be similar to the remaining part of the 3D model used in our study. V_p cross-sections of tomographic models SFV-11 and SFV-08 are shown with equivalent cross-sections of the SCEC reference model in Figure 3. The tomographic cross-sections show slower V_p by a factor of 2 compared to those of the SCEC reference model. Figure 4 shows V_p and V_s cross-sections of model SFV-12 and equivalent cross-section within our subset of the SCEC reference model as well as σ values for both models. Again, we see slower V_p and V_s by factors up to 2 and 1.5, respectively, in the near-surface material for the tomographic model. Notice the similar V_p-structure down to 500 m depth in all three tomographic models. In this study we compare the ground motion generated by our subset of the SCEC reference model and by the model modified with the slower near-surface velocities from tomographic model SFV-12. The synthetics are compared to data from a M_L=5.1 Northridge aftershock.

We also compare the V_p/V_s and σ for both models. The primary goal of this comparison is to determine the differences between the two models, estimate the effects of those differences on the ground motion, and ultimately refine velocities in the near-surface of the latest SCEC reference model. This procedure could potentially improve ground motion estimates in the SFV. We compare the accuracy of the seismic response in terms of amplitude for Northridge aftershock 3147406 (M_L=5.1) (taken from Bonilla *et al.,* 1997). The choice of this event was based on its location within the model boundaries, its relatively large size, and its shallow depth. Stronger earthquakes at shallow depth generally excite the near-surface material more than events at depth, and the ground motion probably includes significant energy less than 1 Hz due to its relatively large size. The 1-Hz limit is introduced by computational considerations. Table 1 lists the hypocentral parameters of this event. Focal parameters given by the Caltech database are duplicated in our model. Table 2 lists the coordinates of the corresponding stations, their instrument characteristics, and the general geology of each site. Table 3 shows the events recorded by each station. Unfortunately, we are unable to compare the synthetics and the data in terms of travel time since the absolute travel times of the event used are unknown.

Numerical Method and Basin Model

We use a 3D fourth-order staggered-grid finite-difference method (Olsen, 1994) to propagate wave motion from a point-source or extended fault through a model of the SFV subsurface. This algorithm is derived from the three-dimensional first-order equations of Newton's

law and Hooke's law (Aki and Richards, 1980):

$$\begin{aligned} \rho(\mathrm{x})\ \dot{u}_i(\mathrm{x},t) &= \tau_{ij,j}(\mathrm{x},t) + F_i(\mathrm{x},t), \\ \dot{\tau}_{ij}(\mathrm{x},t) &= \lambda(\mathrm{x})\delta_{ij}e_{kk} + 2\mu(\mathrm{x})e_{ij}, \\ \dot{e}_{ij}(\mathrm{x},t) &= \tfrac{1}{2}(\tfrac{\partial u_i}{\partial x_j} + \tfrac{\partial u_j}{\partial x_i}), \end{aligned} \tag{1}$$

where $i, j = 1, 2, 3$, Einstein notation is used, τ_{ij} is the stress tensor, $\mathbf{u}$ is the particle velocity vector in three dimensions, λ is the lame's constant, ρ is the density, μ is the shear modulus, F_i is the *ith* component of the source, and the "dot" designates time differentiation. A coarse-grained viscoelasticity approach (Day, 1998) is used to calculate the anelastic attenuation (Q) which is implemented with stress relaxation independently for both P and S waves using a standard linear solid. The equations of motion are solved using a staggered grid as indicated in Figure 5. The focal mechanism, moment, and depth of the aftershock used in the modeling are listed in Table 1. We use a stability criteria, determined by the equation

$$\tfrac{dt}{dx} V^{\max} \leq C', \tag{2}$$

where C' is a constant about 0.6 for 2D and 0.45 for 3D staggered-grid finite-difference schemes, $V^{\max}$ the maximum phase velocity, dx the grid spacing, and dt the time step. We used five points per minimum wavelength, i.e.

$$\tfrac{V^{\min}}{f^{\max} dx} \geq 5, \tag{3}$$

where $f^{\max}$ is the maximum frequency and $V^{\min}$ the minimum wave velocity, to minimize numerical artifacts in the seismograms.

We extracted a 10 km (East-West) by 10 km (North-South) by 5 km (vertical) subset of the SFV from the latest SCEC reference model that included the hypocenter of event

3147406 (see Table 1), five seismic stations that recorded the event, and all three of the tomographic cross sections (see Fig. 1). Table 4 lists the modeling parameters. The slower V_p and V_s of tomographic model SFV-12 were incorporated into the original model producing a combination model by multiplying the P and S wave velocities in the SCEC subset by the average velocity ratio between the two in the upper 500 m of the sedimentary basin portion of our model. The V_p and V_s ratios used in the modeling are shown in Figure 6. We incorporated the tomographic velocities into the SCEC subset at all sites with $V_p \leq 2$ km/s at 100 m depth, which was used as the criteria for distinction between soil and rock sites. We also compared the response for a point source to that for a 3 x 3 km fault plane with the same focal parameters.

The differences in V_p, V_s, V_p/V_s, and Poisson's ratio (σ) between the SCEC subset and tomographic model SFV-12 are shown in Figures 7, 8, 9, and 10, respectively. The V_p (see Fig. 7) of tomographic model SFV-12 are slower than those of the SCEC subset. The largest differences are seen south of about 4 km at depths of 50 to 350 m where the V_p differ by a factor of two. The two models show similar V_p at depths of 400 m, 450 m, and 500 m. The V_s (see Fig. 8) of tomographic model SFV-12 and the SCEC subset are similar at depths of 50, 100, and 400 m. The V_s of SFV-12 are significantly slower at depths of 150 to 350 m but faster at depths of 450 and 500 m. Notice also that the V_s in the SCEC subset is constant from 200 m to 500 m, 50 m increments. The V_p/V_s ratio (see Fig. 9) of SFV-12 is lower than that of the SCEC subset by a factor of two just south of about 4 km at depths of 50 m and 100 m and significantly lower to a depth of 400 m at which they become higher between roughly 2-6 km. Poisson's ratio values (see Fig. 10) for SFV-12 are significantly lower than those of the SCEC subset to a depth of 300 m at which they become fairly consistent.

In the following we use ground motion parameters defined as:

1) The peak particle velocity measured at location (x, y) for the kth component is defined as

$$PGV_k(x, y) = MAX(|\ \dot{u}_k\ (x, y, t)|), \tag{4}$$

where $\dot{u}_k\ (x, y, t)$ is the velocity time history for the kth component, and MAX indicates the maximum value of $|\ \dot{u}_k\ (x, y, t)|$ for all time t.

2) The cumulative kinetic energy per unit volume for the kth component is given as

$$CKE_k(x, y) = \frac{1}{2}\rho(x, y) \int \dot{u}_k^2\ (x, y, t)dt, \tag{5}$$

where $\rho(x, y)$ is the density, and the limits of integration are over the time interval of the simulation. We then take ratios of the two distributions of ground motion parameters that we want to compare.

Effect of Low Near-Surface Velocities

Velocity snapshots of the M_L=5.1 Northridge aftershock for the subset of the SCEC reference model and combination model are shown in Figures 11 and 12, respectively. The effect of the lower P and S velocities from tomographic model SFV-12 are demonstrated in the velocity snapshots of the combination model (Fig. 12), which show slower wave propagation and stronger reverberations in comparison to the response of subset of the SCEC reference model. The PGV and CKE ratios between the SCEC subset and the original combination

model (produced using the extended source) are shown in Figure 13. These plots clearly show that modifying the SCEC subset with (both) the slower P and S velocities from tomographic model SFV-12 affect the ground motion–particularly on the vertical component. Similarly, Figure 14 shows the PGV and CKE ratios between the SCEC subset and the combination model [only V_p changed]. Clearly, the slower P velocities incorporated from tomographic model SFV-12 affect the ground motion–particularly on the vertical component. Figure 15 shows that Q affects the ground motion significantly in very close proximity to the fault.

Comparison of Simulations to Data

We attempt to reproduce the observed seismograms as accurately as possible. Before 3D simulations were compared to data 1) the accelerograms of the data were integrated to obtain the particle velocities recorded at each station, 2) the data were resampled to the time step of the synthetics, and 3) both data and synthetics were bandpass filtered between 0.5 and 1.0 Hz. The data used for comparison (taken from Bonilla *et al.,* 1997) was already calibrated and highpass filtered at 0.5 Hz. The instrument response had already been removed.

First, we carried out 1 Hz 2D sensitivity simulations using a 19.425 km long profile along North-South (see Fig. 1) that intersected the SCEC subset and included tomographic cross-section SFV-12 and the hypocenter of event 3146983 (M_L=4.2). Table 5 lists the hypocentral parameters of this event. The minimum V_s were clamped at 300, 400, and 500 m/s, respectively. The slower V_s from tomographic model SFV-12 were then superimposed on the upper 500 m of the model producing a combination model. We also carried out simulations with and without Q. The results (Fig. 16) show that the soft soils and sediments

of the SFV basin tend to significantly amplify the particle velocities. The maximum peak velocities decreased slightly as the slower V_s were eliminated. As expected, the peak velocities of the combination model increased in the sediments as frequency decreased, suggesting the importance of slow V_s in the near-surface material when performing waveform modeling of a sedimentary basin. The largest effects are seen south of about 10 km, where the SFV basin deepens. The clamping of the minimum velocities is seen to have very small effects on the ground motion simulated in the SCEC model due to the relatively high near-surface velocities here. Q is seen to reduce the maximum peak velocities by a factor of 2 for the combination model due to the relatively slow near-surface velocities here.

We compare our point-source and fault plane synthetic seismograms to three-component records of the M_L=5.1 event. From our point-source simulation, seismograms produced from the SCEC subset showed poor fit to the data. The synthetics for the combination model showed some agreement with sites CSNR and CWHP (vertical components), which are located above the sedimentary basin in our model. Although the seismograms of the combination model show more reverberations and a duration increased by a factor of 2 at some sites, the synthetics lack the complexity of peaks and reverberations seen in the data.

First, we examine the synthetics of the M_L=5.1 aftershock on an extended 3 km by 3 km fault compared to a point-source. Figure 17 shows synthetic seismograms generated within the SCEC subset for point-source and fault plane simulations. From the extended fault simulation (Fig. 18), the synthetic seismograms showed overall fairly good fit to data, with enhanced P and S agreement at stations BRCY (E-W component), CWHP (N-S component), and RESB (E-W component) and good agreement in general at stations CWHP (E-W component), and JFPP (all components). The synthetics generated in the combination model

(Fig. 19) also showed an overall fit to data, with very good P and S agreement at stations BRCY (E-W component), CWHP (N-S component), and RESB (E-W component), and improved fit at station CSNR (N-S and E-W components). Differences between the synthetics generated from the SCEC subset model and those generated by the combination model are shown in Figure 20. Although the differences were not extensive, the seismograms from the combination model do show a slight increase in duration in the vertical components and slightly higher peak velocities in general at most sites. We also examined the effect of Q in our combination model (Figure 21). Seismograms for both models were very similar at four of the five stations, showing no significant differences with or without Q. At station CSNR, however, the removal of Q increased the peak particle velocities on all three components.

To better understand how slow velocities in the near-surface material affect ground motion, we simulated wave propagation within four more combination models using the extended source. First, we modified the near-surface material of the original SCEC subset with only the V_p from tomographic model SFV-12. Seismograms computed for this combination model showed very little deviation from those from the original SCEC subset (Fig. 22). We then incorporated the slower velocities of SFV-12 into the entire model down to 500 m depth. This combination model generated synthetics with a degraded fit to data compared to that for the synthetics from the model where just the soil sites were changed. In the third model we increased the depth of the near-surface material, modifying all of the soil sites (i.e. $V_p \leq$ 2 km/s) by the ratios in Figure 6 down to 750 m depth. For the fourth model we increased the V_p for what we originally considered a soil site, modifying the near-surface material of the original SCEC subset with the slower velocities from tomographic model SFV-12 for $V_p \leq$ 2.5 km/s at 100 m depth (compared previously for $V_p \leq 2$ km/s at 100 m depth). However,

both of these models generated synthetics with a degraded fit to data.

Discussion

Clearly, the V_p and V_s incorporated from tomographic model SFV-12 are significantly slower than those of the SCEC subset (refer to Fig.'s 7 and 8). Figure 14 demonstrates that V_p in the near-surface material ($\leq$ 500 m) of the SFV basin does affect the ground motion, even though its effects are not seen in the seismograms produced at the five stations (Fig. 22). Furthermore, the lower V_s incorporated from SFV-12 did expectedly produce slightly better fit for traces at the five stations (see Fig.'s 18 and 19 for comparison), showing more reverberations and higher peaks. Based on the differences in V_p and V_s between the SCEC subset and tomographic model SFV-12, we estimate that both V_p and V_s need to be reduced in the material $\leq$ 500 m; however, further work is needed to determine a precise depth. Our inability to obtain a better P and S wave fit in our synthetic seismograms when compared to the data at all five sites suggests that the latest version of the SCEC reference model is not complex enough to reproduce the duration and peaks produced by the M_L=5.1 Northridge aftershock on some components (see Fig. 18) within our area of study (see Fig. 1). Inclusion of the slower V_p and V_s from tomographic model SFV-12 does improve the fit slightly, however the synthetic seismograms still lack some complexity seen in the data.

Conclusions

Our 3D simulations of ground motion in a subset of the SCEC southern California reference 3D seismic velocity model, version 2.0, in the SFV, suggests that the model is not complex enough to reproduce the 1-Hz duration and peaks of an actual Northridge aftershock event. Inclusion of the slower V_p and V_s from tomographic model SFV-12 in the near-surface material increased peak ground velocities and cumulative kinetic energies by more than a factor of two in localized areas of the model; however, the lower velocities did not have a significant effect on the ground motion at five seismic stations where synthetics were compared to data.

Acknowledgments

We are grateful to F. Bonilla for providing the calibrated aftershock data. This study was supported by the Southern California Earthquake Center (SCEC) Summer Undergraduate Research Internship Program.

References

[1] Aki, K. and P. G. Richards. *Quantitative Seismology Theory and Methods* (Vol. 1). New York: W. H. Freeman and Company, 1980.

[2] Aki, K. and P. G. Richards. *Quantitative Seismology Theory and Methods* (Vol. 2). New York: W. H. Freeman and Company, 1980.

[3] Alex, C. M. and K. B. Olsen (1998). Lens effect in Santa Monica? *Geophys. Res. Lett.*, **25**, 3441-3444.

[4] Anderson, J. G., Y. Lee, Y. Zeng, and S. M. Day (1996). Control of strong motion by upper 30 meters, *Bull. Seism. Soc. Am.*, **86**, 1749-1759.

[5] Bonilla, L. F., J. H. Steidl, G. T. Lindley, A. G. Tumarkin, and R. J. Archuleta (1997). Site amplification in the San Fernando Valley, California: Variability of site-effect estimation using the S-wave, coda, and H/V methods, *Bull. Seism. Soc. Am.*, **87**, 710-730.

[6] Boore, D. M. (1972). A note on the effect of simple topography on seismic SH waves, *Bull. Seism. Soc. Am.*, **62**, 275-284.

[7] Borcherdt, R. D. and G. Glassmoyer (1992). On the characteristics of local geology and their influence on ground motions generated by the Loma Prieta earthquake in the San Francisco Bay region, California, *Bull. Seism. Soc. Am.*, **82**, 603-641.

[8] Day, S. M. (1996). RMS response of a one-dimensional half-space to SH, *Bull. Seism. Soc. Am.*, **86**, 363-370.

[9] Day, S. M. (1998). Efficient simulation of constant Q using coarse-grained memory variables, *Bull. Seism. Soc. Am.*, **88**, 1051-1062.

[10] Field, E. H., P. A. Johnson, I. A. Beresnev, and Y. Zeng (1997). Nonlinear ground-motion amplification by sediments during the 1994 Northridge earthquake, *Nature*, **390**, 599-602.

[11] Gao, S., H. Liu, P. M. Davis, and L. Knopoff (1996). Localized amplification of seismic waves and correlation with damage due to the Northridge earthquake: Evidence for focusing in Santa Monica, *Bull. Seism. Soc. Am.*, **86**, S209-S230.

[12] Graves, R. W., A. Pitarka, and P. G. Somerville (1998). Ground Motion Amplification in the Santa Monica Area: Effects of Shallow Basin Edge Structure, *Bull. Seism. Soc. Am.*, **88**, 1224-1242.

[13] Hartzell, S., E. Cranswick, A. Frankel, D. Carver, and M. Meremonte (1997). Variability of site response in the Los Angeles urban area, *Bull. Seism. Soc. Am.*, **87**, 1377-1400.

[14] Joyner, W. B., R. E. Warrick, and T. E. Fumal (1981). The effect of Quaternary alluvium on strong ground motion in the Coyote Lake, California, earthquake of 1979, *Bull. Seism. Soc. Am.*, **71**, 1333-1349.

[15] Khain, K. R., S. K. Datta, and A. H. Shah (1991). Amplification of obliquely incident seismic waves by cylindrical alluvial valley of arbitrary cross-sectional shape. Part II. Incident SH and Rayleigh waves, *Bull. Seism. Soc. Am.*, **81**, 346-357.

[16] Magistrale, H., S. Day, R. W. Clayton, and R. Graves (2000). The SCEC southern California reference 3D seismic velocity model version 2, *Bull. Seism. Soc. Am.*, in press.

[17] Olsen, K. B. (1994). Simulation of three-dimensional wave propagation in the Salt Lake Basin, *Ph. D. Thesis*, University of Utah.

[18] Olsen, K. B., R. J. Archuleta, and J. R. Matarese (1995). Three-dimensional simulation of a magnitude 7.75 earthquake on the San Andreas fault, *Science*, **270**, 1628-1632.

[19] Olsen, K. B. and R. J. Archuleta (1996). Three-dimensional simulation of earthquakes on the Los Angeles fault system, *Bull. Seism. Soc. Am.*, **86**, 575-596.

[20] Olsen, K. B. (2000). Site amplification in the LA basin from 3-D modeling of earthquakes, *Bull. Seism. Soc. Am.*, in press.

[21] Pattelena, T. H., D. Okaya, and N. Godfrey (1998). Velocity structure of the near-surface San Fernando Valley from tomographic inversion of active-source data, *SCEC Summer Undergraduate Research Internship Program.*

[22] Su, F., K. Aki, T. Teng, Y. Zeng, S. Koyanagi, and K. Mayeda (1992). The relation between site amplification factor and surficial geology in central California, *Bull. Seism. Soc. Am.*, **82**, 580-602.

[23] Vidale, J. E. and D. V. Helmberger (1988). Elastic finite-difference modeling of the 1971 San Fernando, California, earthquake, *Bull. Seism. Soc. Am.*, **78**, 122-141.

[24] Wright, T. L. (1991). Structural geology and tectonic evolution of the Los Angeles basin, California, in *Active Margin Basins*, K. T. Biddle (Editor), *AAPG Mem.*, **52**, 35-134.

Tables

Table 1

Northridge Aftershock Event 3147406 Parameters

Date	HHMMSS	M_L	Lat	Long	Depth(km)	*Strike*°	*Dip*°	*Rake*°
94/01/29	11:20:35.60	5.1	34.3053	-118.5770	1.59	330	80	-20

Table 2

Instrument Characteristics of Stations

Station	Lat	Long	Array	Sensor	Logger	Samples/sec	Geol
BRCY	34.3060	-118.5790	NORT	L4C,FBA23	16-bit RT72A-02	250	T
CSNR	34.2395	-118.5314	NORT	L4C,FBA23	16-bit RT72A-02	250	Q
CWHP	34.2590	-118.5730	NORT	L4C,FBA23	16-bit RT72A-02	250	Q
JFPP	34.3120	-118.4960	NORT	L4C,FBA23	16-bit RT72A-02	250	Q
NWHP	34.3880	-118.5332	NORT	L4C,FBA23	16-bit RT72A-02	250	Q
RESB	34.2968	-118.5507	NORT	L4C,FBA23	16-bit RT72A-02	250	T
SFMI	34.2708	-118.4612	NORT	L4C,FBA23	16-bit RT72A-02	250	Q

Table 3

Events Recorded by Each Station Used in This Study

Event ID	BRCY	CSNR	CWHP	JFPP	NWHP	RESB	SFMI
3146983		X	X	X	X	X	X
3147406	X	X	X	X		X	

Table 4

3-D Viscoelastic Modeling Parameters

Parameter	
Grid spacing (m)	50
Number of east-west grid points	260
Number of north-south grid points	260
Number of vertical grid points	130
Number of time steps	10,000
Time step (sec)	0.0034
Rise time (sec)	0.45
Minimum V_s (m/s)	250
Minimum V_p (m/s)	433
Maximum V_p (m/s)	6375
Density (g/cm^3)	1.7
Q_s	$0.1 \cdot V_s$ (m/s)
Minimum source frequency (Hz)	0
Maximum source frequency (Hz)	1.0

Table 5

Northridge Aftershock Event 3146983 Parameters

Date	HHMMSS	M_L	Lat	Long	Depth(km)	$Strike^\circ$	Dip°	$Rake^\circ$
94/01/28	20:09:53.39	4.2	34.3703	-118.5022	4.00	215	35	100

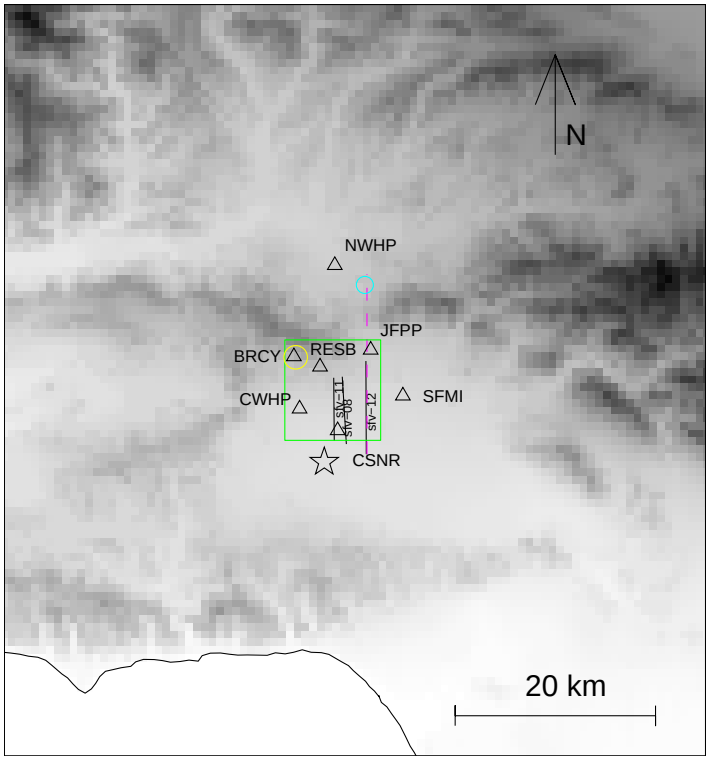

Figure 1: Regional map of the San Fernando Valley and vicinity. Event epicenters are represented by circles and recording sites by triangles. The yellow circle represents the M_L=5.1 event used in the 3D modeling. The smaller cyan circle represents the M_L=4.2 event used in the 2D sensitivity simulations. The green rectangle represents the subset extracted from the SCEC reference model used in our 3D modeling. The dashed magenta line represents the 2D model profile. Tomographic profiles (from Pattelena *et al.,* 1998) are shown as solid black lines. Northridge mainshock epicenter is represented by the star.

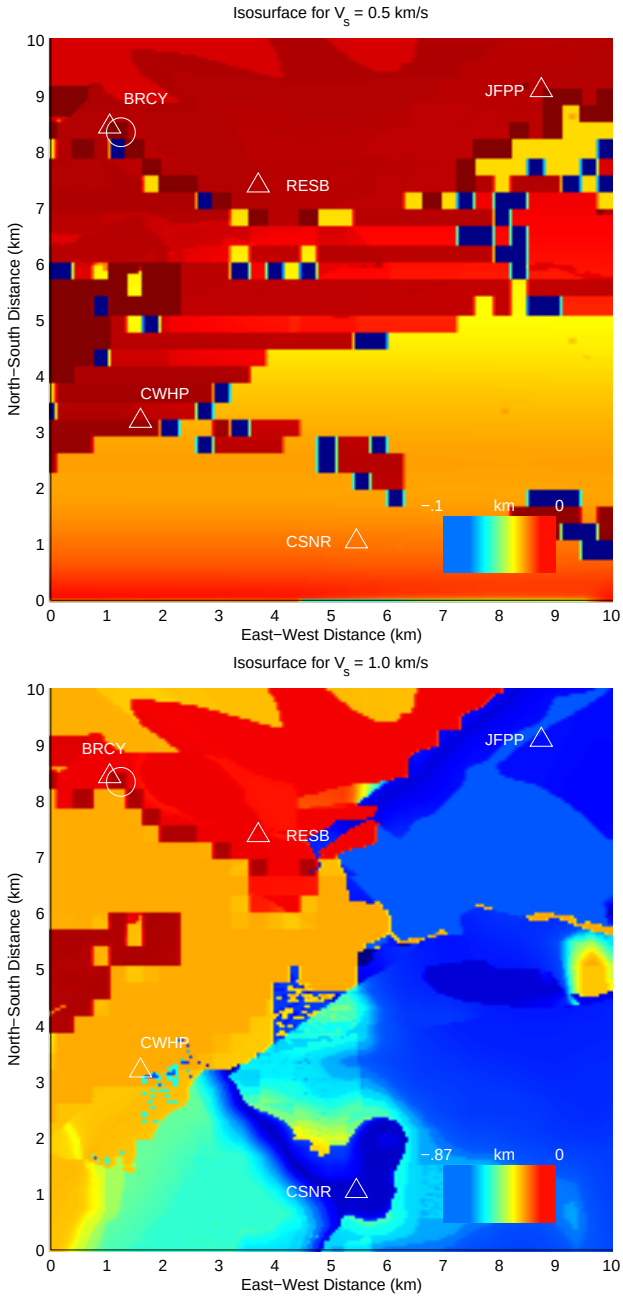

Figure 2: Isosurfaces for V_s=500 m/s (top) and V_s=1000 m/s (bottom) extracted from the SCEC 3D seismic velocity model, Version 2, produced by Magistrale *et al.* (2000).

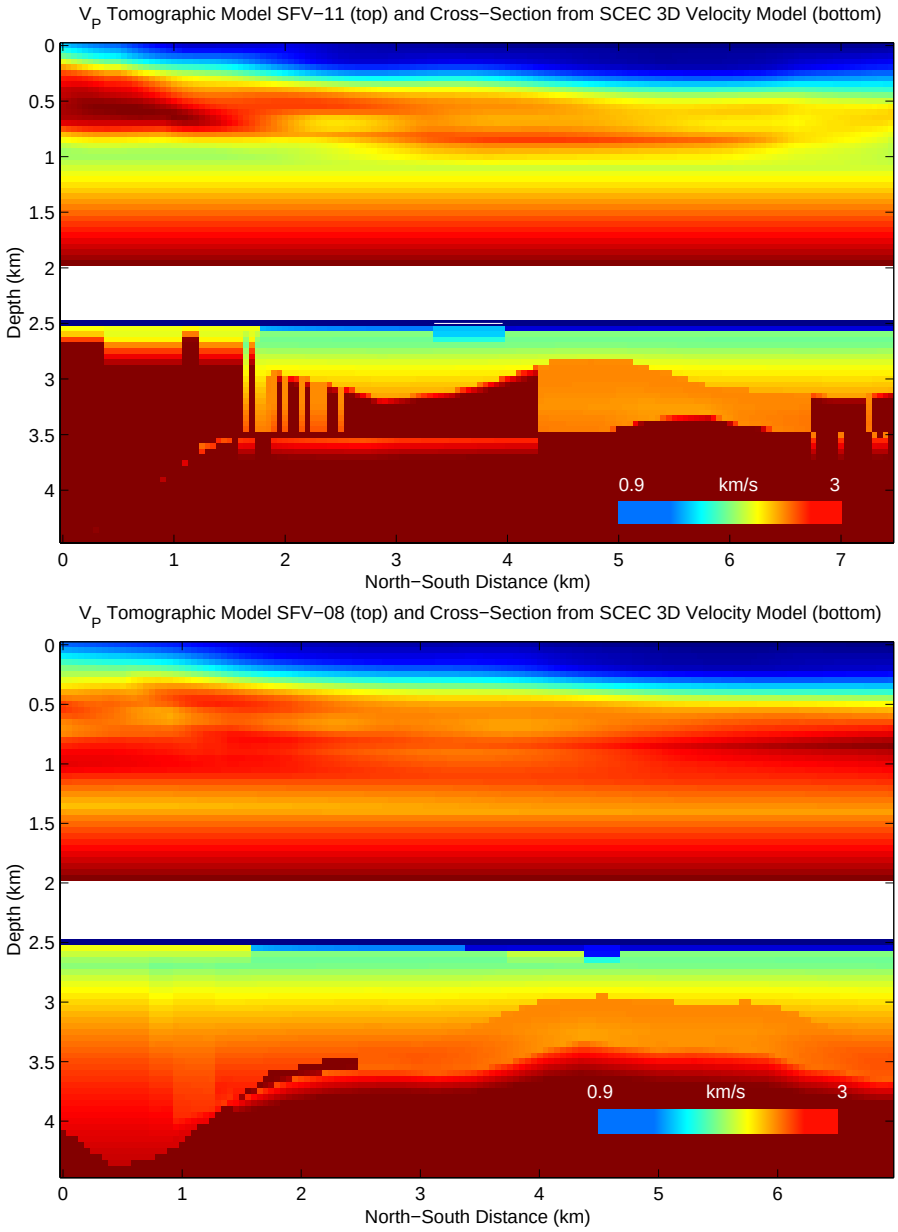

Figure 3: V_p models for tomographic cross-sections SFV-11 (top) and SFV-08 (bottom) (taken from Pattelena *et al.*, 1998) along with equivalent cross-sections within our subset of the SCEC reference model. Accuracy of tomographic models extends to about 500 m depth.

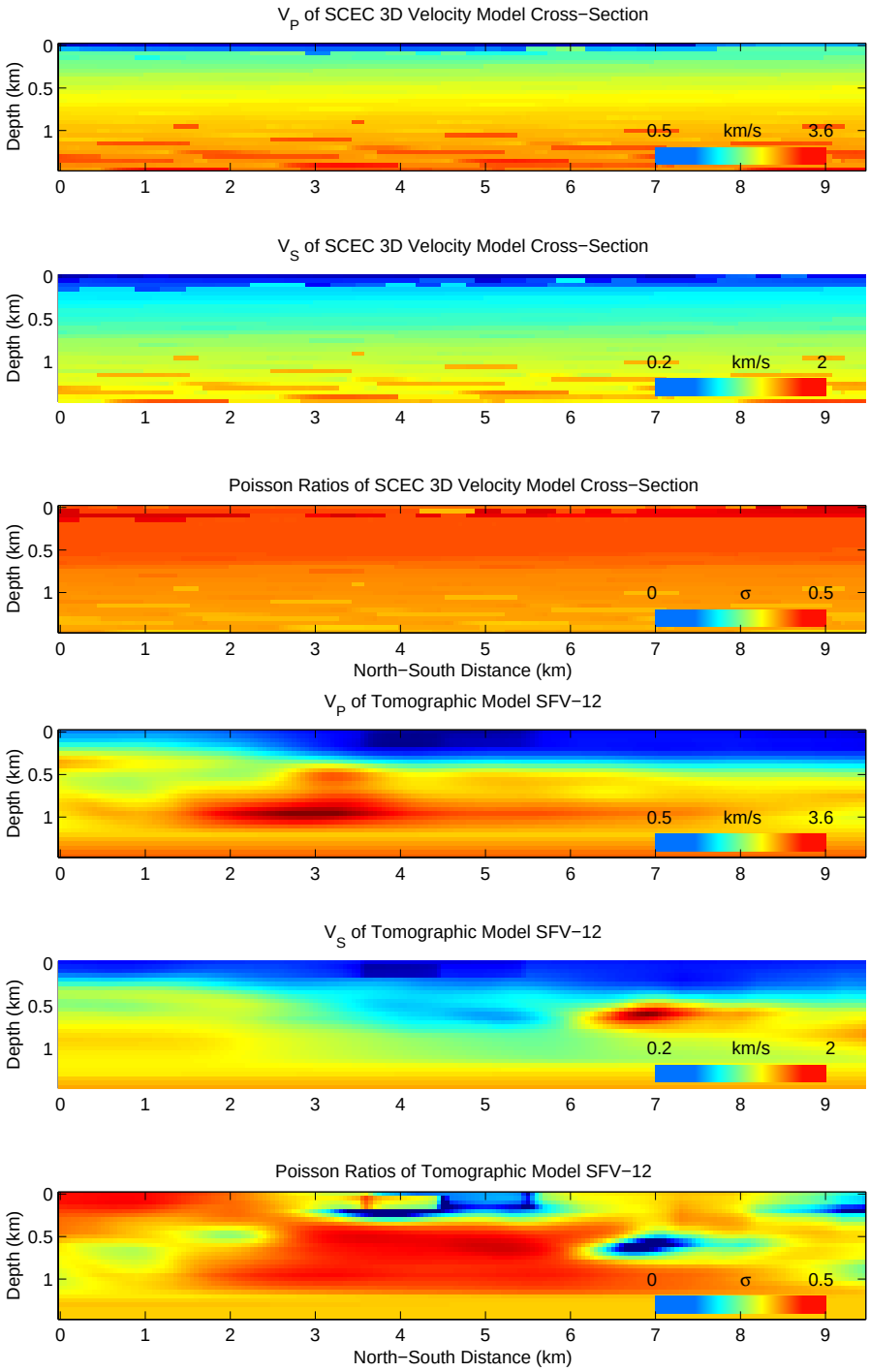

Figure 4: V_p and V_s and Poisson's ratio (σ) models for tomographic cross-section SFV-12 (taken from Pattelena *et al.*, 1998) along with equivalent cross-section within our subset of the SCEC reference model. Accuracy of tomographic models extends to about 500 m depth.

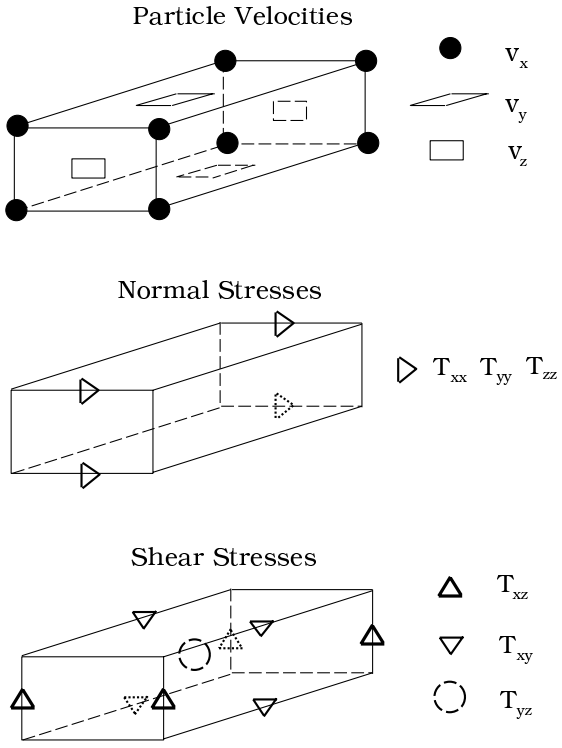

Figure 5: Positioning of particle velocities and normal and shear stresses using a staggered grid.

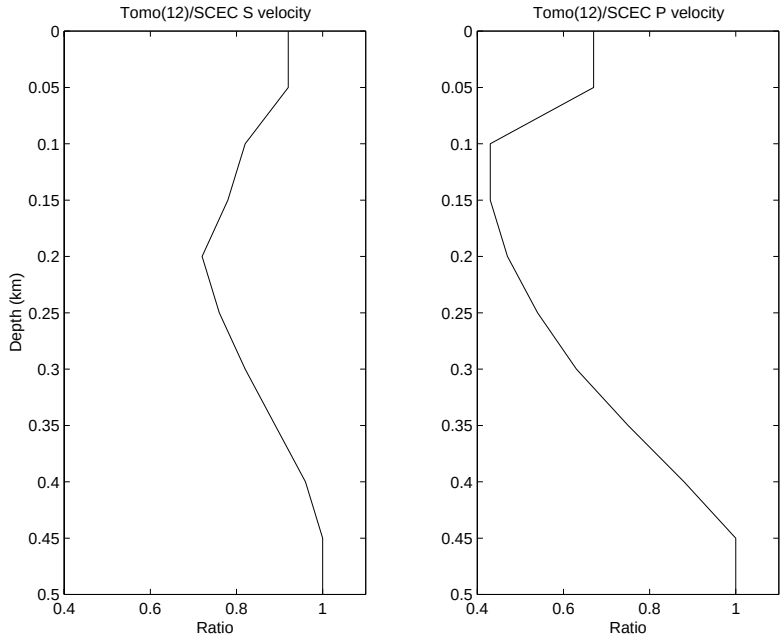

Figure 6: V_s (left) and V_p (right) ratios used in the modeling between tomographic model SFV-12 and our subset of the SCEC reference model.

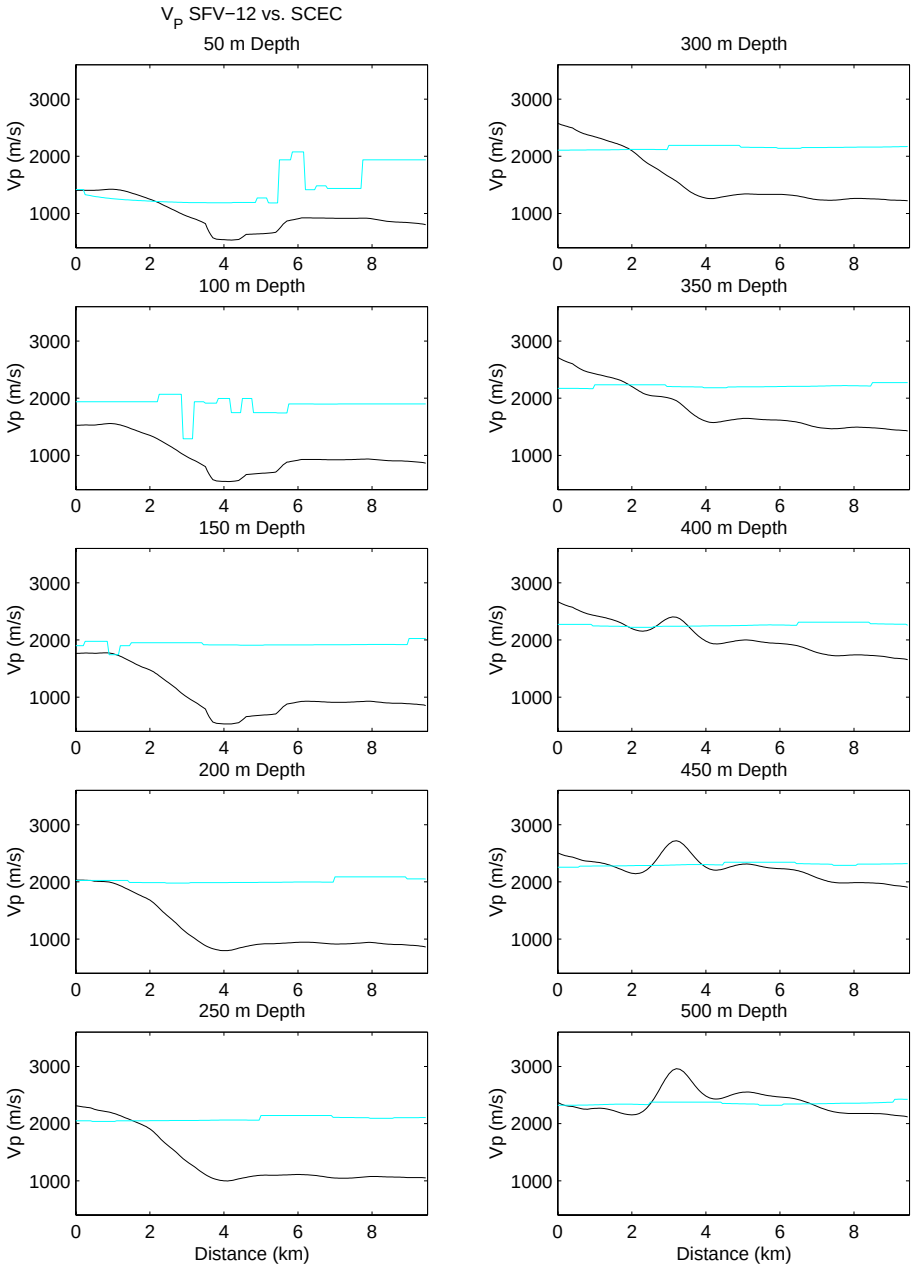

Figure 7: Comparison of V_p from the tomographic model SFV-12 (black) and the subset of the SCEC reference model (cyan).

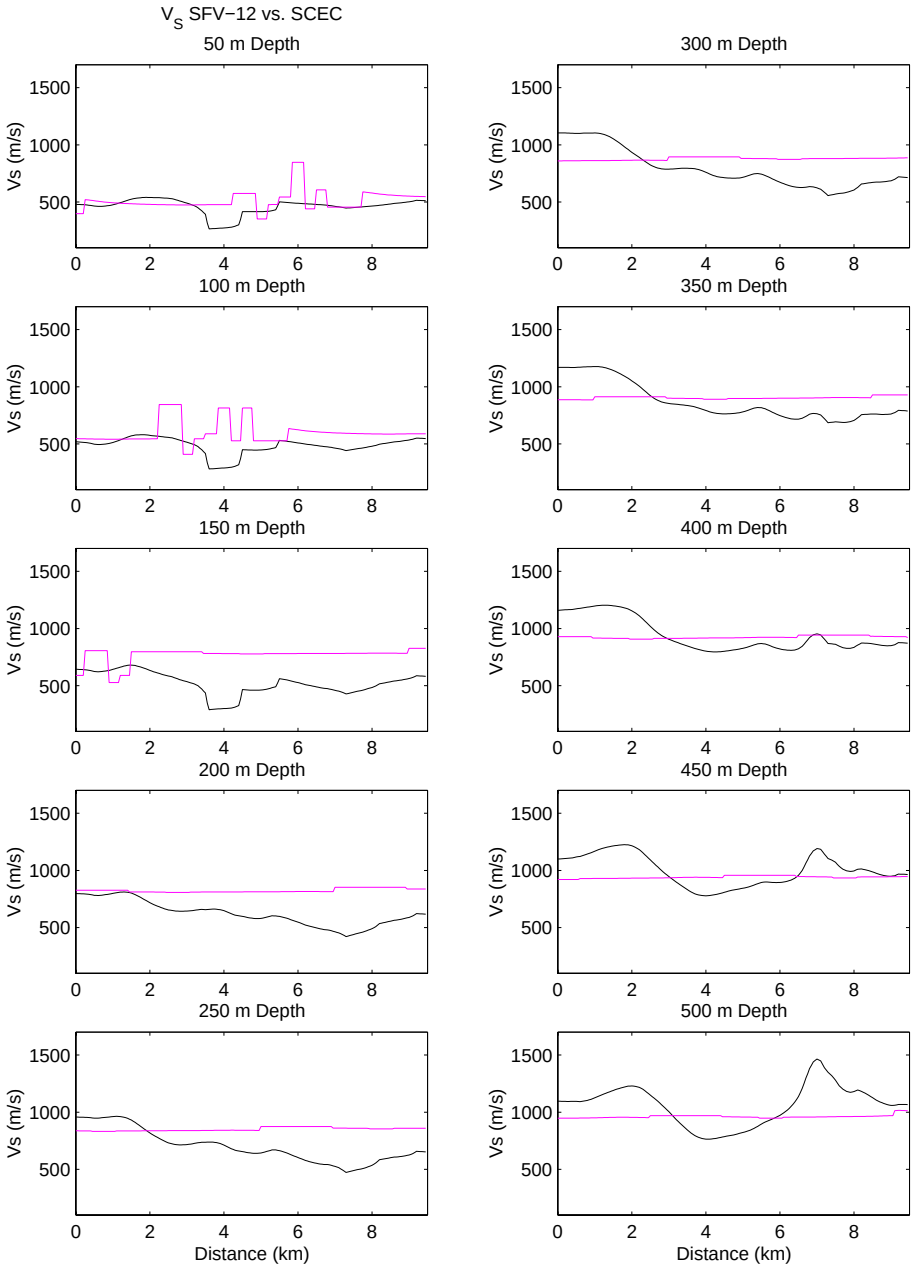

Figure 8: Comparison of V_s from the tomographic model SFV-12 (black) and the subset of the SCEC reference model (magenta).

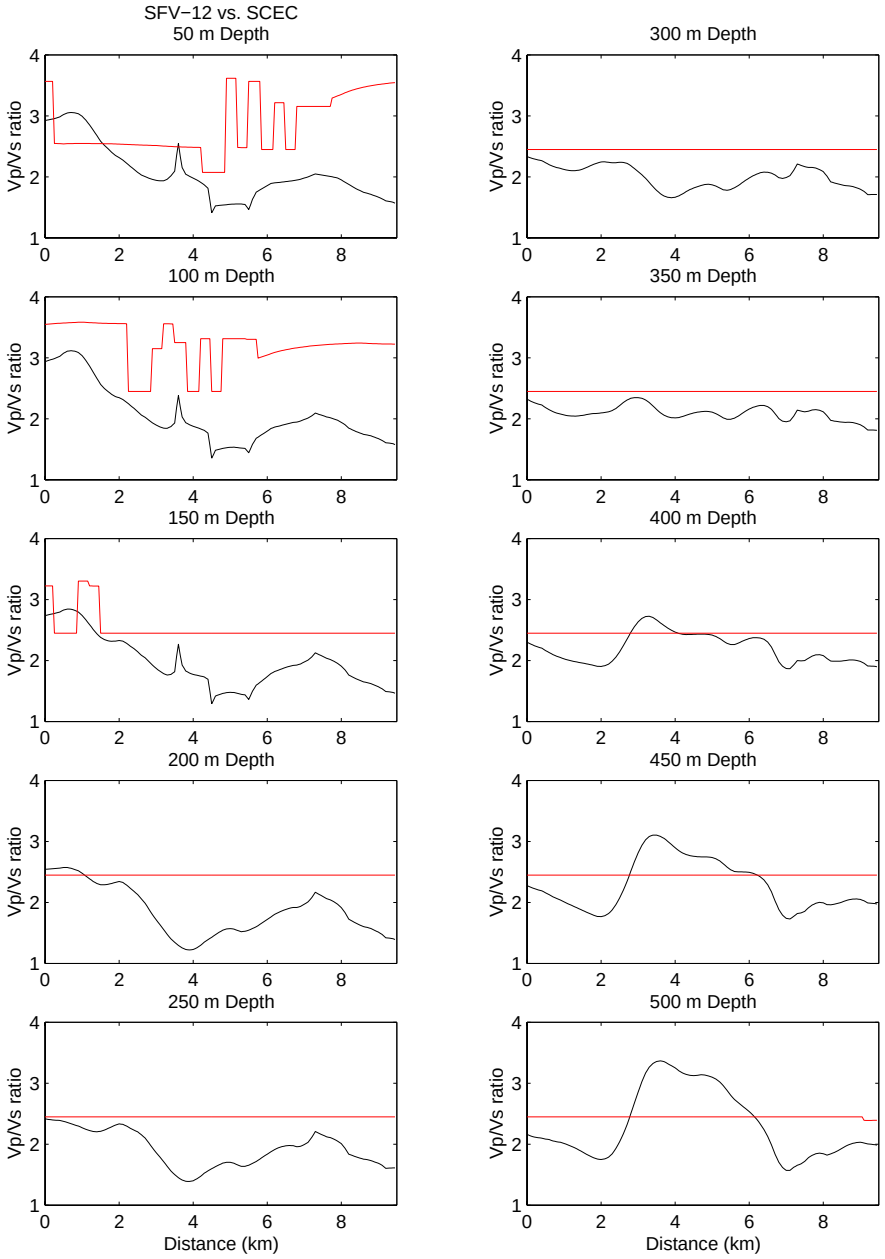

Figure 9: Comparison of V_p/V_s ratio from the tomographic model SFV-12 (black) and the subset of the SCEC reference model (red).

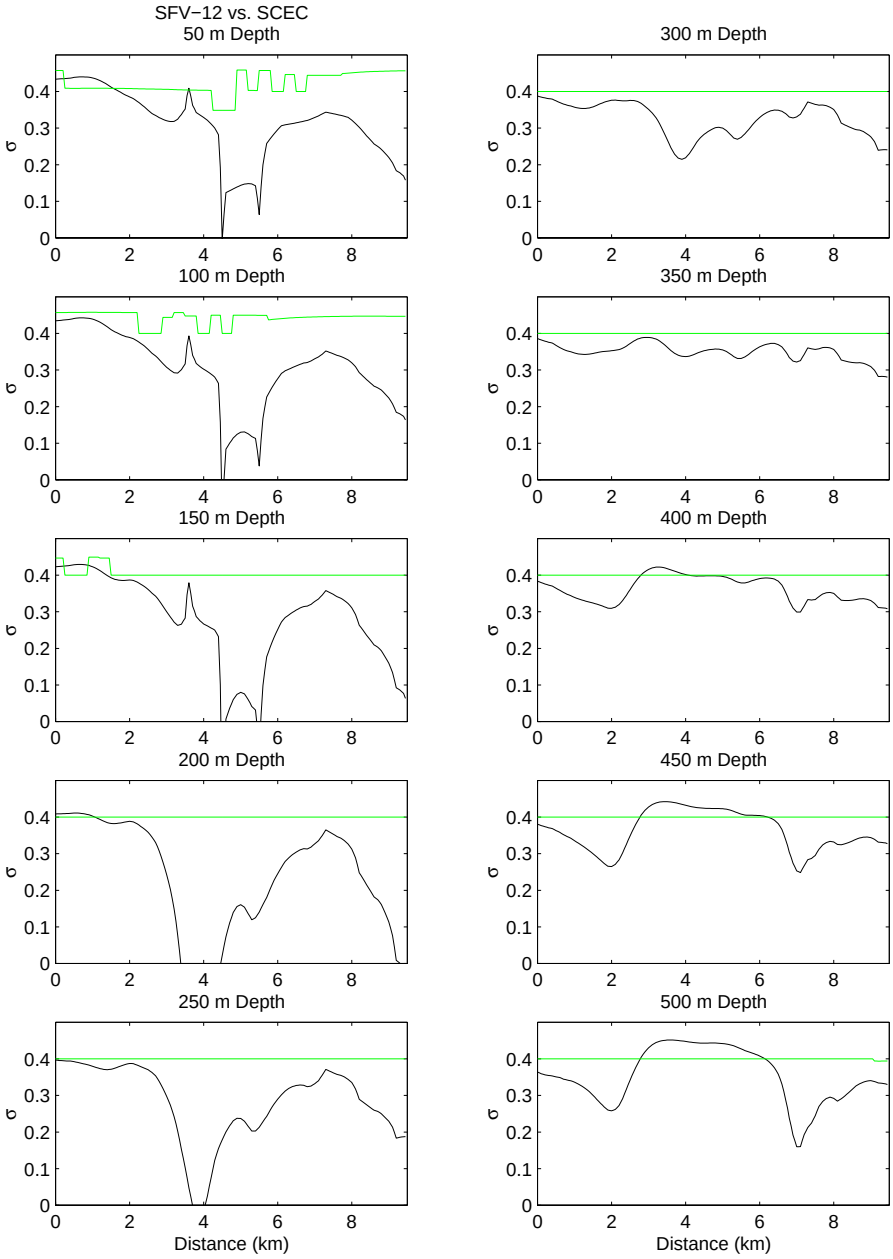

Figure 10: Comparison of Poisson's ratio from the tomographic model SFV-12 (black) and the subset of the SCEC reference model (green).

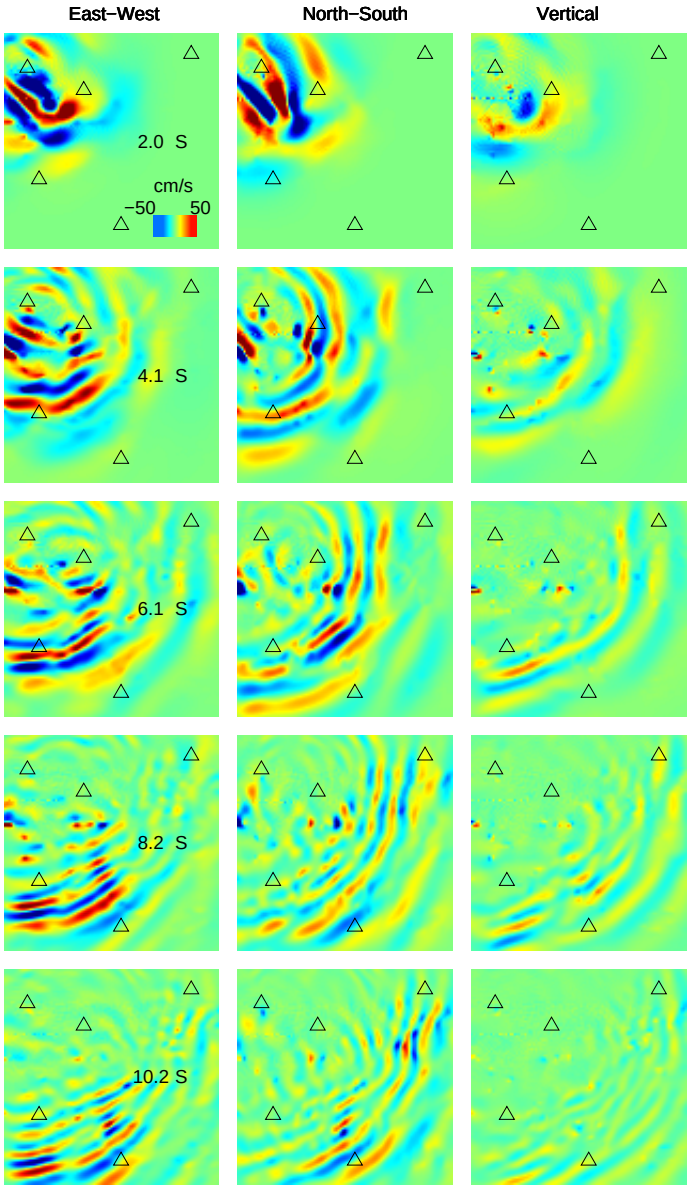

Figure 11: Velocity snapshots for the subset of the SCEC reference model.

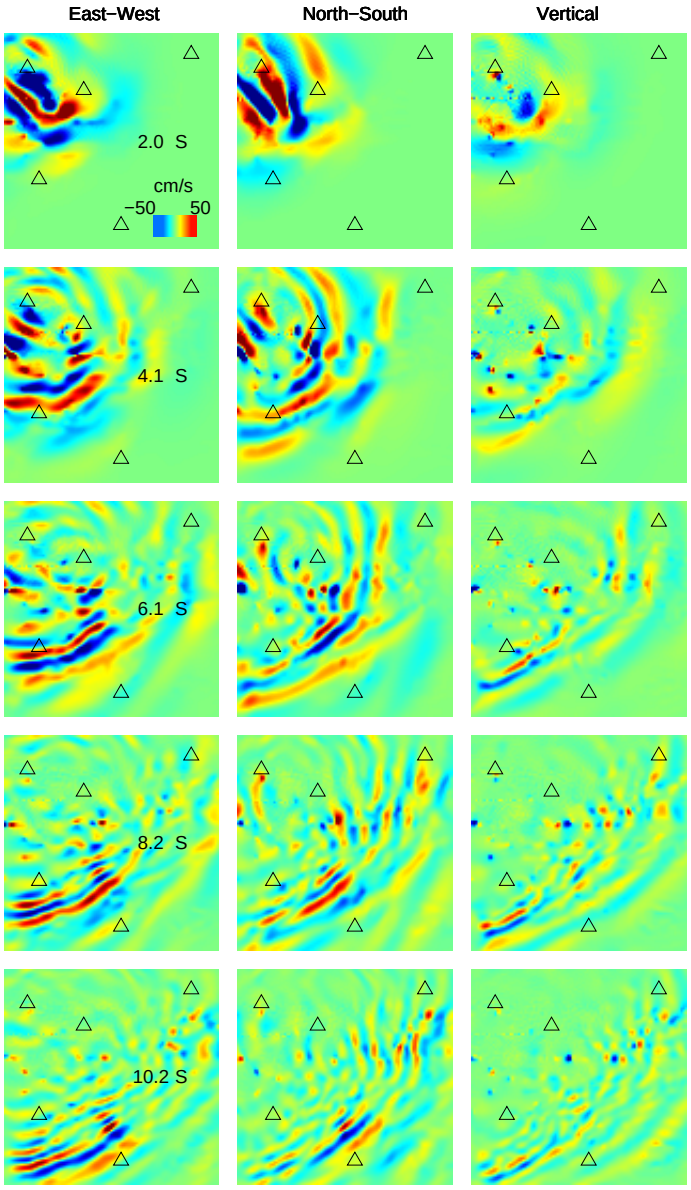

Figure 12: Velocity snapshots for the combination model.

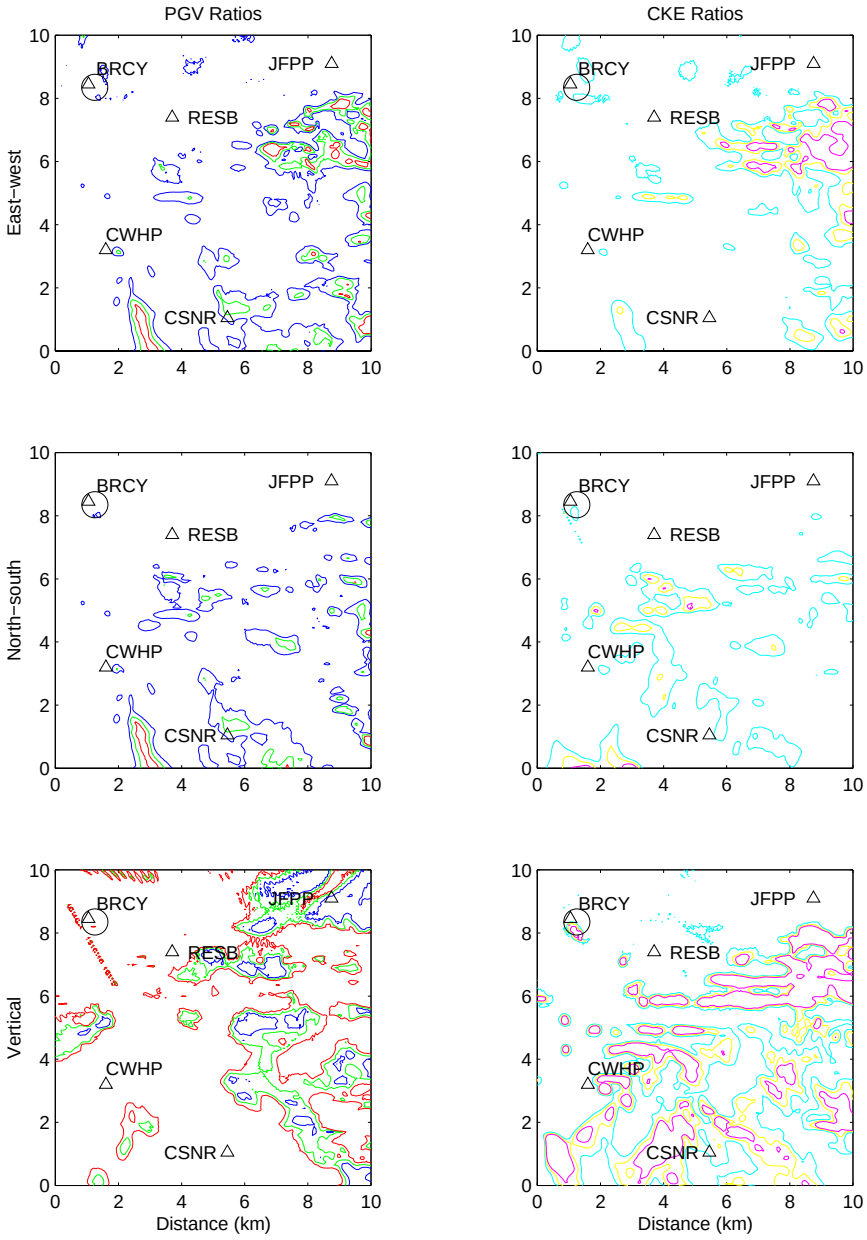

Figure 13: Ratios of peak ground velocity (PGV) and cumulative kinetic energy (CKE) for the combination model and the subset of the SCEC reference model. For PGV, a ratio of 1.25 is blue, 1.5 is green, and 1.75 is red. For CKE, a ratio of 1.5 is cyan, 2 is yellow, and 2.5 is magenta.

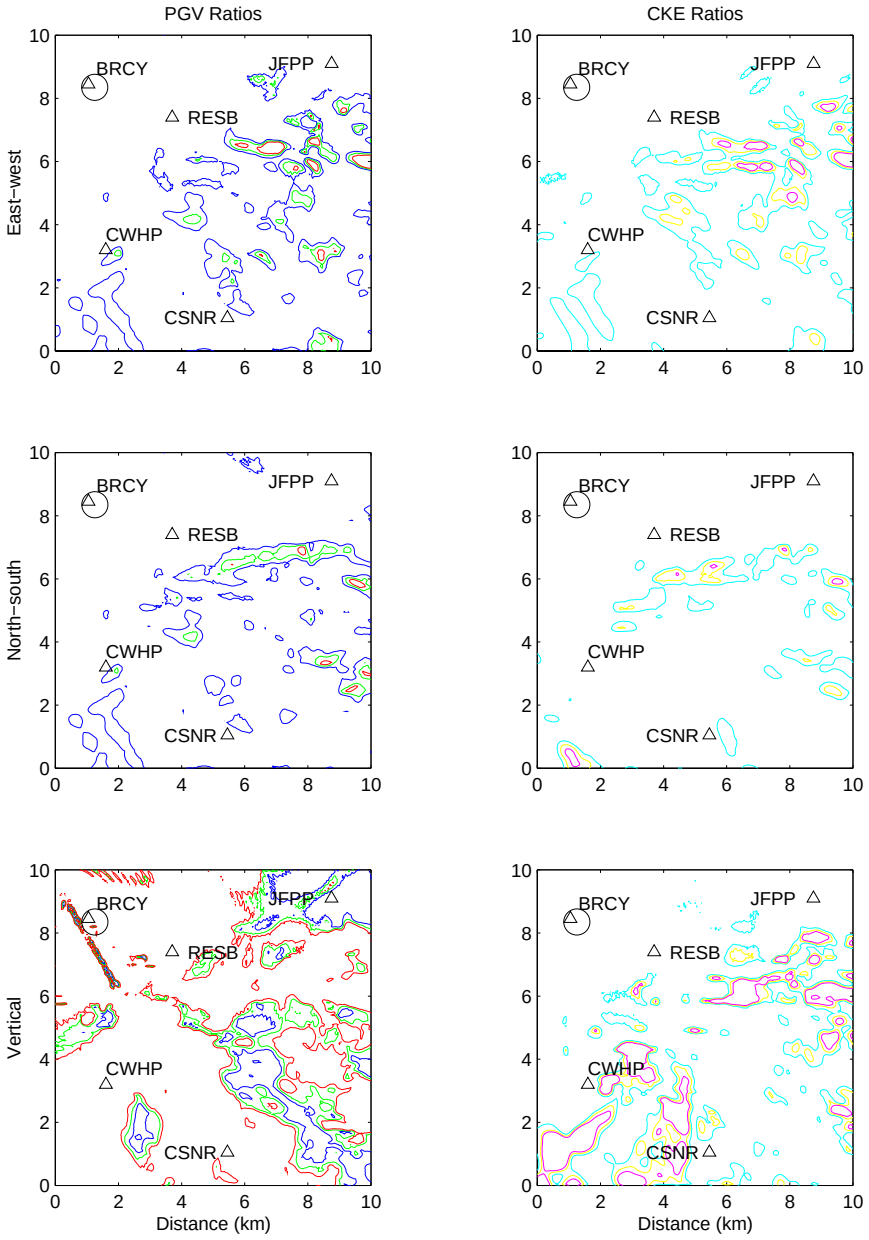

Figure 14: Ratios of peak ground velocity (PGV) and cumulative kinetic energy (CKE) for the combination model where only V_p was modified and the subset of the SCEC reference model. For PGV, a ratio of 1.25 is blue, 1.5 is green, and 1.75 is red. For CKE, a ratio of 1.5 is cyan, 2 is yellow, and 2.5 is magenta.

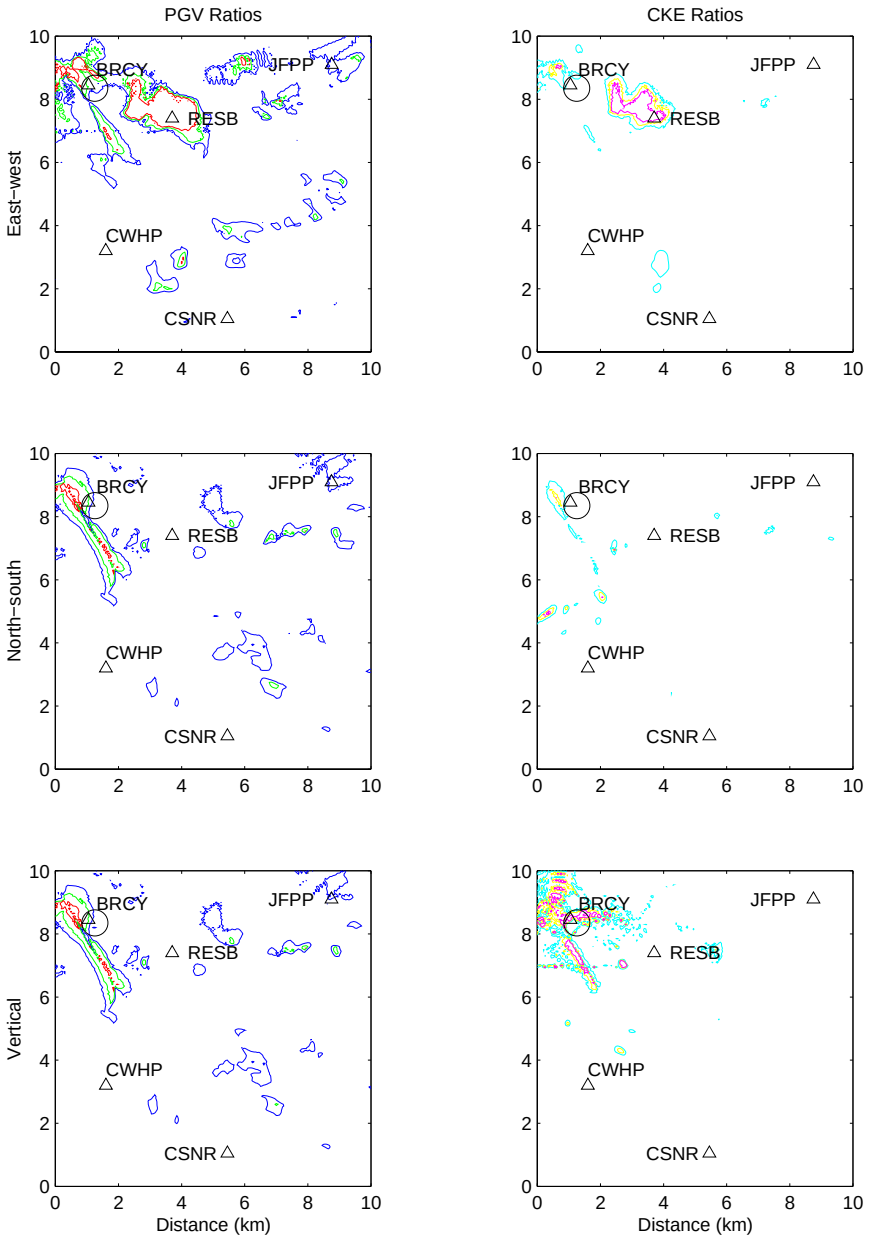

Figure 15: Ratios of peak ground velocity (PGV) and cumulative kinetic energy (CKE) for the combination model without Q and with Q. For PGV, a ratio of 1.25 is blue, 1.5 is green, and 1.75 is red. For CKE, a ratio of 1.5 is cyan, 2 is yellow, and 2.5 is magenta.

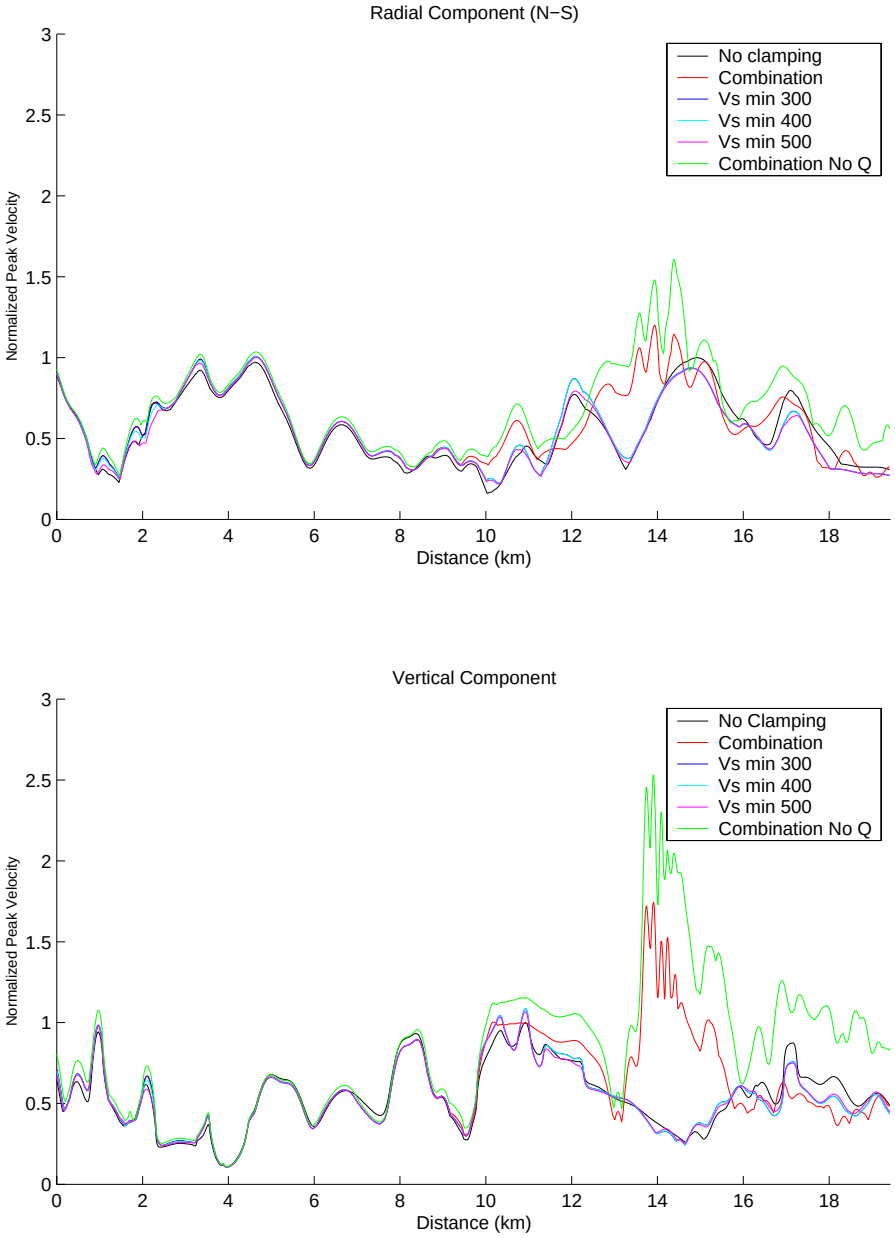

Figure 16: Maximum normalized peak velocities for 2D sensitivity models. Distance is North-South with North to the reader's left.

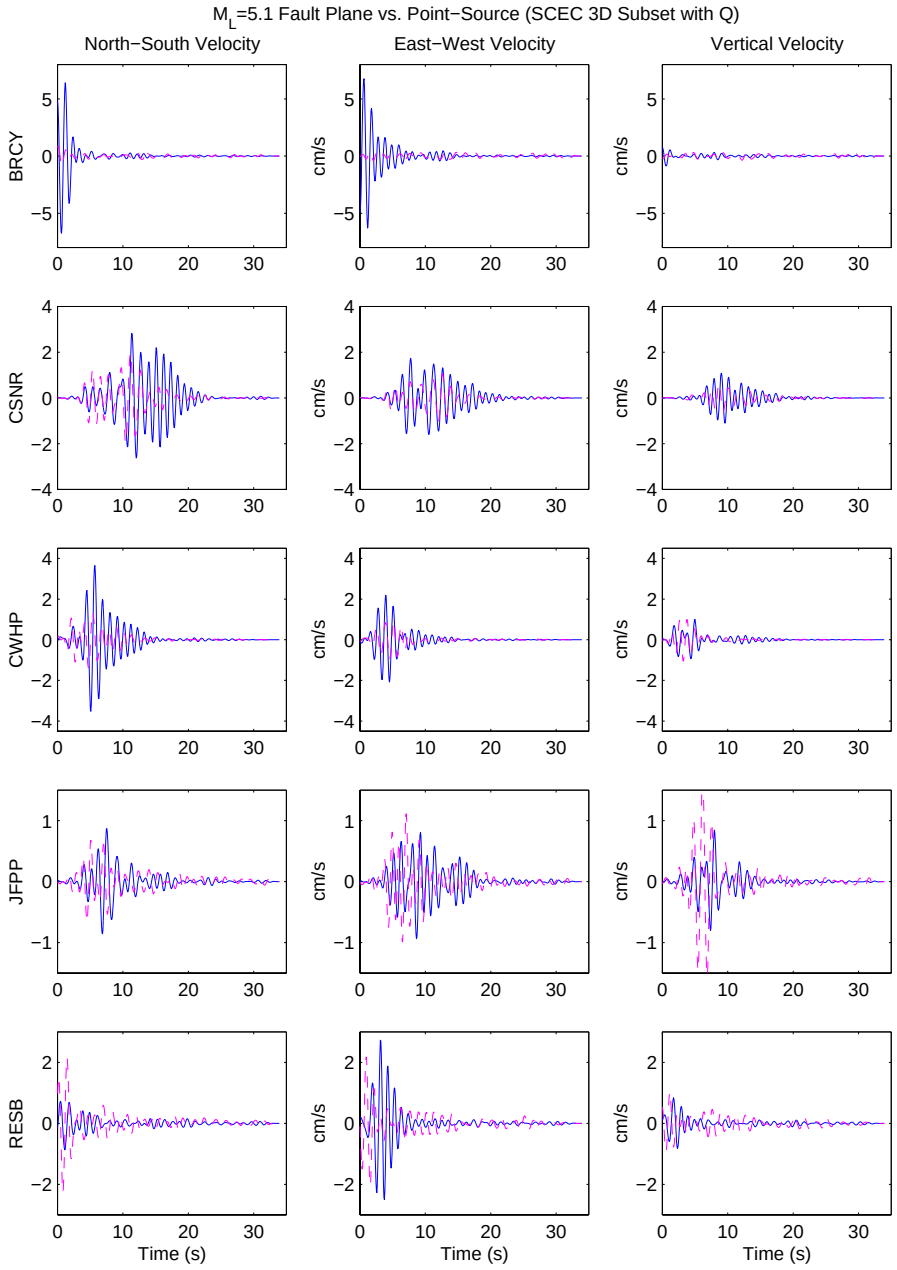

Figure 17: Comparison of synthetic seismograms for simulations using an extended fault (blue) a point-source (dashed magenta).

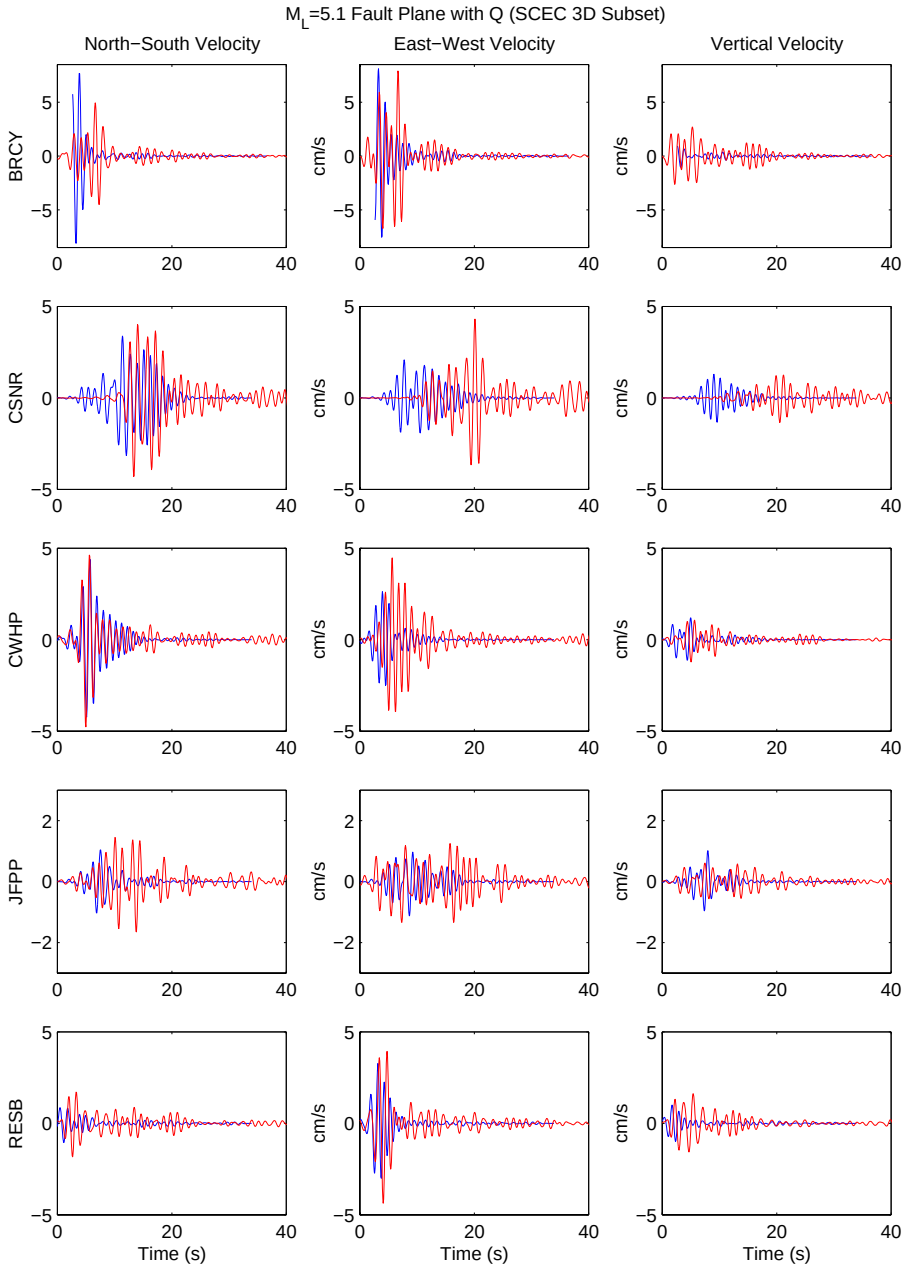

Figure 18: Comparison of synthetic seismograms from the subset of the SCEC reference model (blue) to data (red).

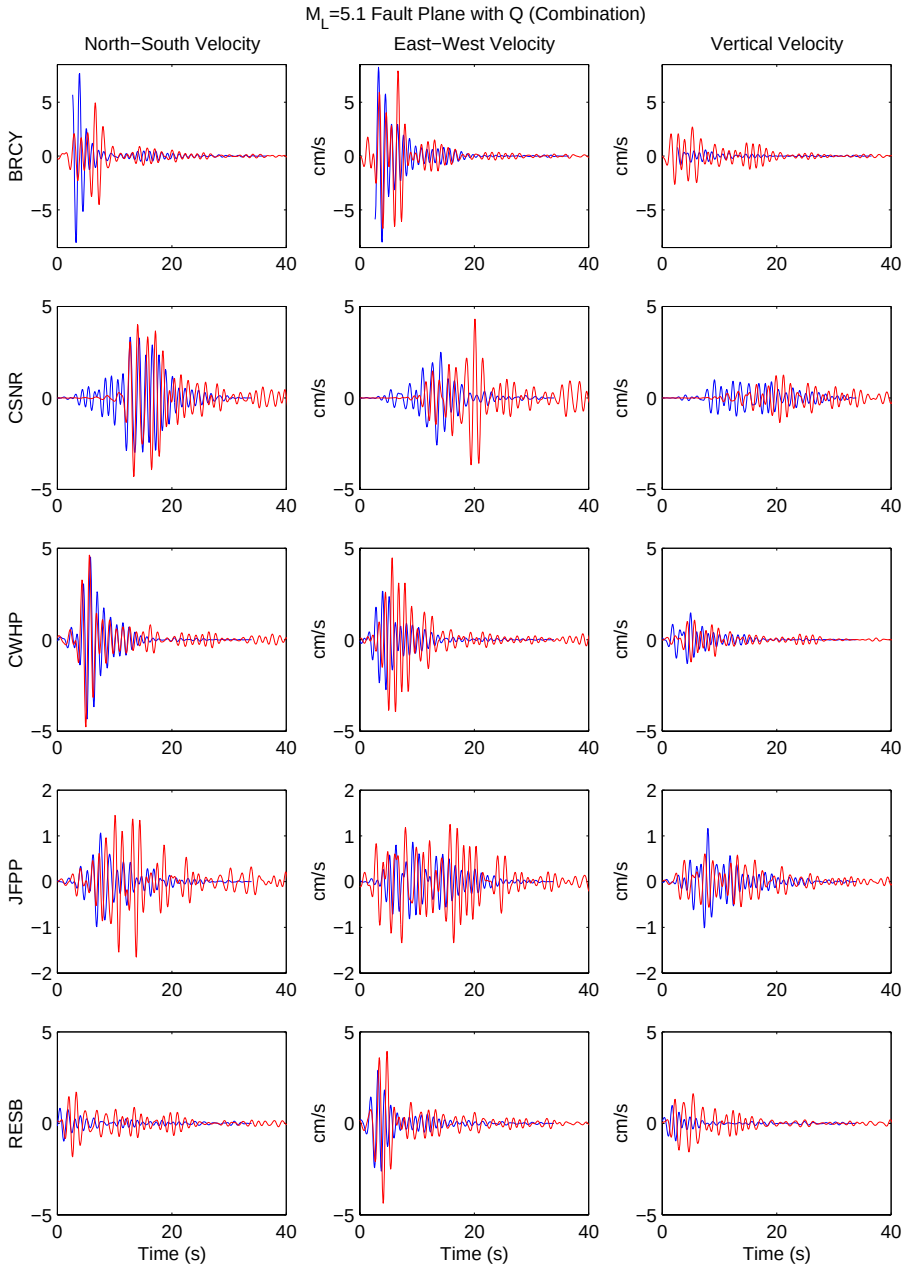

Figure 19: Comparison of synthetic seismograms for the combination model (blue) to data (red).

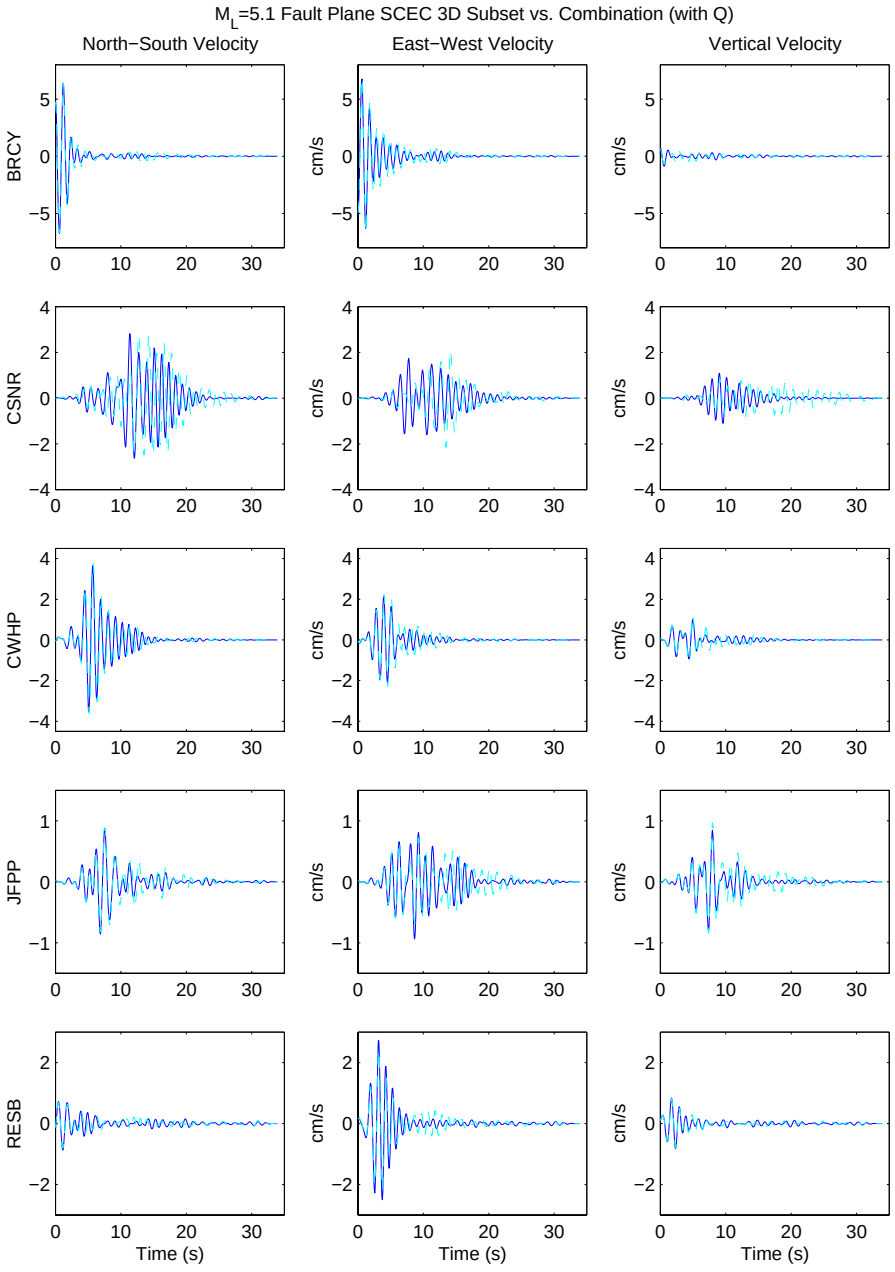

Figure 20: Comparison of synthetic seismograms from subset of the SCEC reference model (blue) to those from the original combination model (dashed cyan).

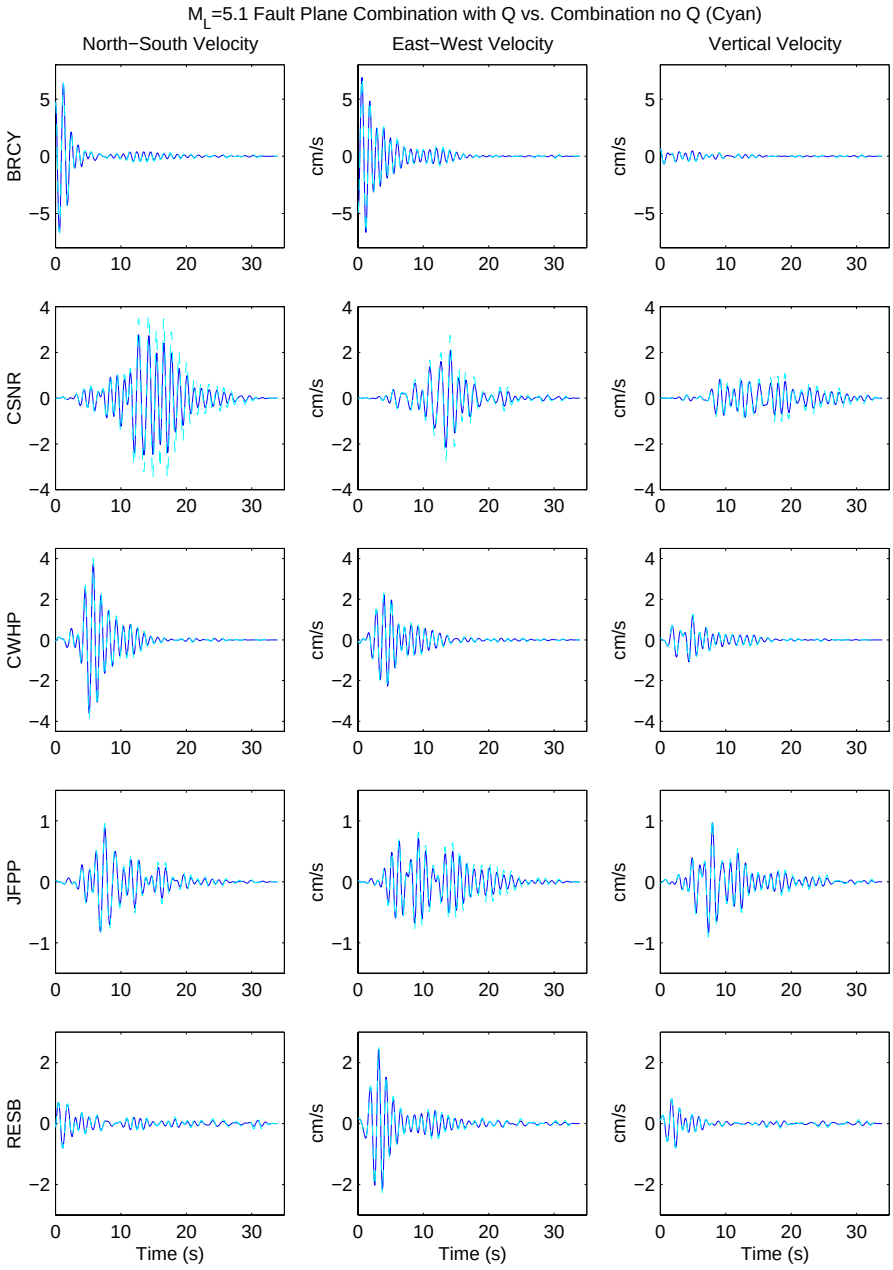

Figure 21: Comparison of synthetic seismograms plotted for the original combination model with Q (blue) and no Q (dashed cyan).

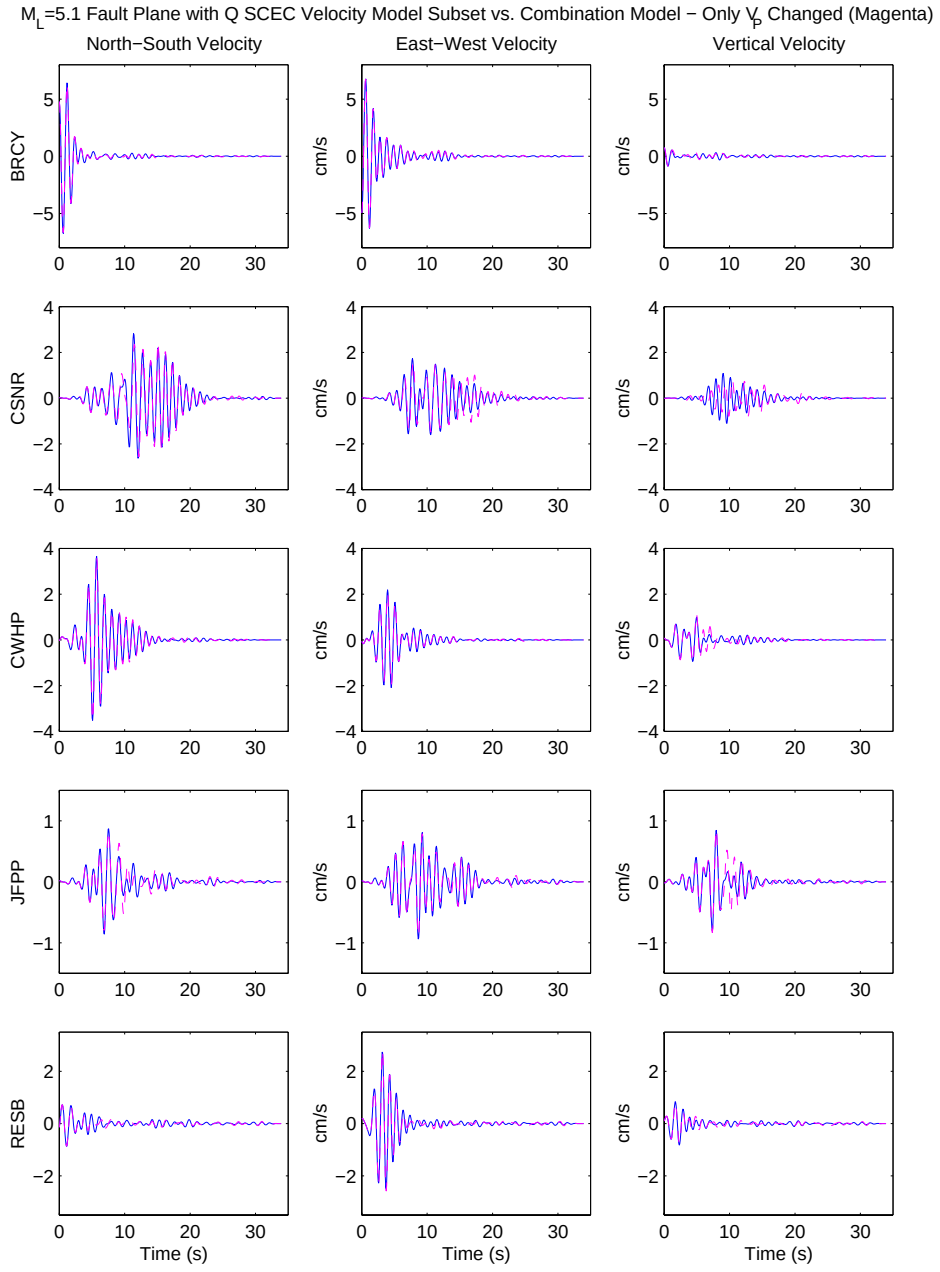

Figure 22: Comparison of synthetic seismograms from the subset of the SCEC reference model (blue) to those for the combination model - only V_P changed (dashed magenta).